Attributes affecting the Accuracy of a Batch Least Square Orbit Determination using Semi-analytical Satellite Theory

Srinivas J. Setty
PhD Student, DLR/GSOC, Wessling, Germany
Paul J. Cefola
University of Baffalo and Consultant in Space-flight Mechanics and Astrodynamics
Hauke Fiedler
Head of Space Situational Awareness Group, DLR/GSOC, Wessling, Germany
Juan Felix San Juan Diaz
Professor at the Department of Mathematics and Computing
Universidad de La Rioja, Logroño, Spain

ABSTRACT

The study presents an analysis of the orbit determination process for maintenance of the space object catalogue. After quantifying the uncertainties in optical and radar measurements, the second part of the study presents the error within the mean element orbit determination procedure. A batch least square orbit determination method which makes use of the Draper semi-analytical satellite theory and its partial derivatives is tested for its correctness under catalogue maintenance conditions. Different attributes, which could affect the performance of such an orbit determination method, are identified and examined with real and simulated observations. In conclusion, the factors which limit the practical accuracies of the orbit determination procedure are discussed.

1. INTRODUCTION

To date, there have been over 5,160 launches and approximately 200 known satellite break-ups [17]. These factors have caused space operations within the Earth bound orbital regions to become an area of concern and increased interest. Wiedemann et al., [22] estimate that the objects orbiting the Earth with size of 1 cm and greater have exceeded 700,000. According to another report [17], the number of objects in orbit which are 10 cm and greater, also known as hazardous objects, are over 17,000. Analysing the publicly available NORAD catalogue (downloaded on May 20, 2016), these objects are scattered around in different orbital heights, eccentricities, and inclinations. Figure 1 shows the objects distribution in different mean element spaces.

In order to protect the operational space assets, it has become inevitable to track these space objects and to maintain a space object catalogue. Such a catalogue will assist the space operations and be useful for a nations' non-civilian purposes. Figure 2 shows the high level process of catalogue maintenance system. Morton et al.,[16] estimate that the US Joint Space Operation Center (JSpOC) performs about 40,000 track and object correlations per day to maintain their catalogue and provide collision warnings. This system requires a few hundred thousands of orbit predictions and determination runs per day. On the other hand, Boikov et al.,[3] state that the Russian Space Surveillance Centre performs about ten million orbit propagations every day to maintain their catalogue. Orbit propagation and orbit determination techniques are integral parts of all nodes of a catalogue maintenance system. In order to compute 10^5 to 10^7 orbit predictions per day, the orbit propagation technique for catalogue maintenance must be computationally efficient and at the same time accurate. Setty et al., [19] performed an analysis on a suitable candidate propagation technique, and suggest that Draper Semi-analytical Satellite Theory (DSST) is a viable option for this task.

Since DSST is a theory based on Generalized Method of Averaging, the propagation is performed in mean-element space. To take complete advantage of the DSST, a least square orbit determination (OD) system has been implemented. In DSST the recovery of short periodic effects are carried out using analytical forms. This indirectly affects the estimation of orbits.

Copyright © 2016 Advanced Maui Optical and Space Surveillance Technologies Conference (AMOS) – www.amostech.com

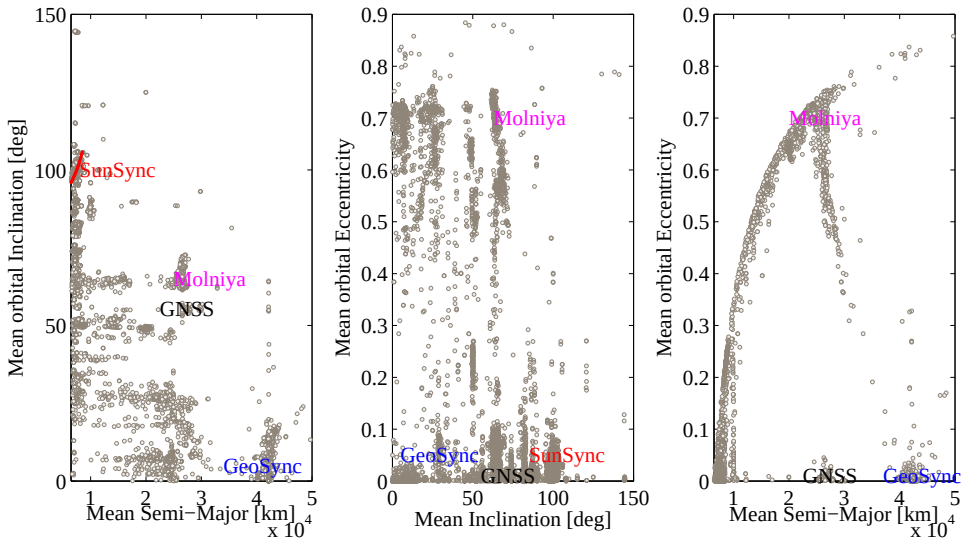

Fig. 1. Space object distribution from NORAD catalogue, dated May 20, 2016, in $(a - e - i)$ orbital space. Main application orbital regions are highlighted with their names

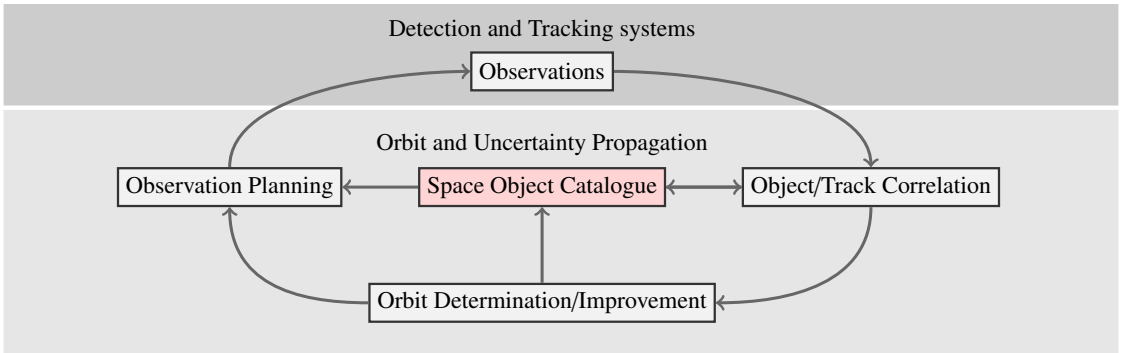

Fig. 2. Elements of Space object catalogue maintenance system

Copyright © 2016 Advanced Maui Optical and Space Surveillance Technologies Conference (AMOS) – www.amostech.com

Figure 3 presents the sensor locations dedicated, contributing, and planned for Space Surveillance and Tracking (SST). The observability of an object depends on its orbit and on the observing station location. Though there are globally spread sensor locations, the inter agency data sharing is still restricted due to national limitations. These factors render the intra agency catalogue maintenance system with very few observations and lower latency. Hence, it calls for an analysis of estimating mean elements used by a semi-analytical method based on available sparse SST observations.

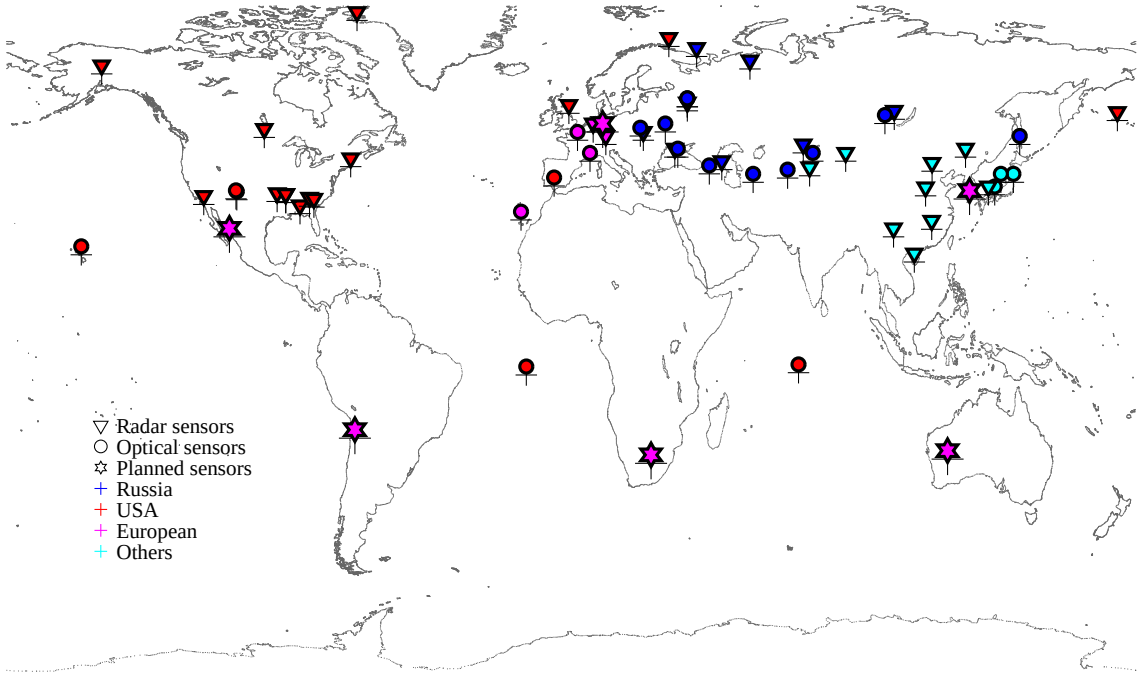

Fig. 3. Dedicated, contributing, and planned sensor locations from different space surveillance programs

Previously, Barker et al., [1] studied the treatment of SST observation errors, their correlations, and force model uncertainty accounting for the accuracy of an estimated orbit. This study employs sensor-by-sensor observation error models using statistical methods. Barker's study was specifically dedicated to providing an overview of the complications of geometric dependencies of the observations. Seago et al., [18] present the influence of sparse tracking on the correctness of a sequential estimation technique. The current study is specifically dedicated to analyse the effects of SST observations in terms of quality, quantity, and their time distribution on orbit determination using least square technique.

Section 2 provides a brief introduction to DSST and implemented semi-analytical least square orbit determination method. Readers familiar with the theory can skip the section; the readers interested in prediction and determination accuracy of the standalone version of DSST are directed to refer [19]. Section 3 introduces the most commonly used observation techniques and their accuracies in debris monitoring and tracking modes. Section 4 presents prediction accuracy of the DSST at different altitudes and for extended lengths of propagation intervals. Discussion on the observation attributes and factors influencing accuracy of the estimated mean orbital elements are presented in Section 5. In the end, conclusions and future works are presented.

2. ORBIT DETERMINATION WITH DSST

The Draper Semi-analytical Satellite Theory (DSST) is a precision mean element satellite theory. It was developed at the Draper Laboratory and the Computer Sciences Corporation by a team led by Paul J. Cefola. DSST is a semi-analytical theory expressed in a non-singular equinoctial elements set. Description, implementation, and suitability of the DSST have been previously discussed in [14, 6, 19]. The procedure for making use of a semi-analytical satellite theory within an orbit determination program is discussed in brief.

Copyright © 2016 Advanced Maui Optical and Space Surveillance Technologies Conference (AMOS) – www.amostech.com

A Batch Least Square (BLSQ) orbit determination method is applied extensively in most existing orbit determination systems for catalogue maintenance. The intention of this part of the work is to reduce the computational effort in OD runs; for this purpose we coupled the DSST with the BLSQ orbit determination method. A semi-analytical way of computing partial derivatives for a perturbed object which is compatible with the DSST was formulated by [11]. This section provides a brief insight to the selected part of Green's work.

For a given initial condition of a space object, with state $\boldsymbol{X}_{t_0}$ associated with covariance $\mathbf{P}_{t_0}$ and for available arc of observations, BLSQ provides the best estimate at the epoch state, $\hat{\boldsymbol{X}}_{t_0} = \boldsymbol{X}_{t_0} + \delta\boldsymbol{x}_0$. This is carried out in an iterative process by solving a Normal equation 1.

$$\delta\mathbf{x}_0 = (A^T W A)^{-1} A^T W \mathbf{b} \tag{1}$$

where,

$$\begin{aligned} A &: \text{partial derivative matrix} \\ W &: \text{weighting matrix} \\ \mathbf{b} &: \text{residual vector} \end{aligned}$$

Derivation and preparation of the components of the Normal equation are described in [15]. The partial derivative matrix, A, is usually composed of the 'observation matrix: H' and the 'state transition matrix: Φ' (STM).

$$A = \frac{\partial\alpha(t)}{\partial\mathbf{X}(t)} \cdot \frac{\partial\mathbf{X}(t)}{\partial\mathbf{X}_{t_0}} = H_{t,t} \cdot \Phi_{t,0} \tag{2}$$

$\Phi_{t,0}$ can be computed by finite differencing method or by integrating the variational equations. $\Phi_{t,0}$ provides the slope and direction to the least square system towards convergence. To reach convergence (best estimate) in a smaller number of iterations, one has to include the major perturbing forces while establishing $\Phi_{t,0}$.

Runtime profiling of an OD system showed that computation of the STM is one of the major resource consuming parts of that OD software. The profiling was carried out on a BLSQ program which used the numerical propagator, and the same is assumed to be true for other OD processes. The DSST-OD computes the STM in a semi-analytical fashion, thereby intending to reduce the computational load of the OD.

DSST employs propagation in mean element space while the observations are in osculating space. To map the mean space to the observed osculating space, the STM is further divided into two components, as in Equation 3

$$\Phi = \frac{\partial\mathbf{X}_t}{\partial\underline{\mathbf{c}}(t)} G \tag{3}$$

Here, $\mathbf{X}_t$ represents the osculating positions and velocities and $\underline{\mathbf{c}}(t)$ represents the osculating equinoctial elements at an arbitrary time, t. G represents the perturbed partial derivatives which are expressed as

$$G = \left[\left\{ \frac{\partial\underline{\mathbf{c}}(t)}{\partial\bar{\mathbf{c}}_0} \right\} \left\{ \frac{\partial\underline{\mathbf{c}}(t)}{\partial\underline{\mathbf{p}}} \right\} \right] \tag{4}$$

with $\bar{\mathbf{c}}_0$ as the epoch mean equinoctial elements, and $\underline{\mathbf{p}}$ as the vector composed of the dynamical parameters in the least square estimation. For handling computation in a modular way, G matrix is further expanded as

$$G = [I + B_1][B_2|B_3] + [0|B_4] \tag{5}$$

Copyright © 2016 Advanced Maui Optical and Space Surveillance Technologies Conference (AMOS) – www.amostech.com

with

$$B_1 = \left[\frac{\partial \varepsilon \underline{\eta}_1(\underline{c}_t)}{\partial \overline{c}(t)}\right] \qquad B_3 = \left[\frac{\partial \overline{c}(t)}{\partial \underline{p}}\right]$$
$$B_2 = \left[\frac{\partial \overline{c}(t)}{\partial \overline{c}_0}\right] \qquad B_4 = \left[\frac{\partial \varepsilon \underline{\eta}_1(\underline{c})}{\partial \underline{p}}\right]$$

The B_2 and B_3 matrices are the partial derivatives of the mean elements at arbitrary time w.r.t. epoch time mean elements and solve-for parameters, respectively. The B_1 and B_4 matrices represent the short periodic portion of the semi-analytical partial derivatives, which are computed at observation time intervals.

The B_2 and B_3 matrices are governed by linear differential Equations 6 and 7, and are computed on the mean element integration time grid. For the DSST, this is usually on the order of a half or one day step sizes.

$$\frac{d}{dt}B_2 = CB_2 \text{ with } [B_2]_{t_0} = I \tag{6}$$
$$\frac{d}{dt}B_3 = CB_3 + D \text{ with } [B_3]_{t_0} = [0] \tag{7}$$

with

$$C = \left\{\frac{[d/dt(\overline{c})]}{\partial \overline{c}(t)}\right\} \qquad D = \left\{\frac{[d/dt(\overline{c})]}{\partial \underline{p}}\right\} \tag{8}$$

In Equations 8, the numerator of the right hand side stands for the VOP equations in mean equinoctial elements. Description in [8] provides the detailed discussion about the STM and their properties along with the implementation structure in the GTDS software program.

In Equation 3, the first part of the right hand side, $\frac{\partial \mathbf{X}_t}{\partial \underline{\mathbf{c}}(t)}$, is the two-body partial derivatives, which maps the variations in the equinoctial elements to positions and velocities. Formulation and implementation of two body partials is straight-forward and can be found in [13] and [20].

3. OBSERVATION CHARACTERISTICS

The first part of the space surveillance and tracking system, being the detection of space debris, is achieved by using three basic types of sensors: optical, radar, and space based sensors. Figure 4 shows the schematic representation of different satellite observation methods in use.

Other means for tracking satellites include Global Positioning System (GPS) and Satellite Laser Ranging (SLR) measurements. These are possible only if the satellite carries a GPS receiver or a retroreflector on-board, which limits the detection of new debris and adjunct satellites. If the observations are available from GPS or SLR measurements, they are used for catalogue maintenance. Currently, optical and radar systems are employed for the purpose of space surveillance. Optical sensors measure the visible energy emitted or reflected by objects, while radar sensors measure high-frequency radio waves reflected by objects. These sensors are based either on ground or could be on a satellite (space based).

Copyright © 2016 Advanced Maui Optical and Space Surveillance Technologies Conference (AMOS) – www.amostech.com

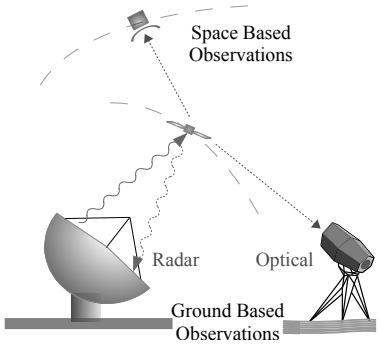

Fig. 4. Representation of general space object observation methods

The following section presents the observation methods employed at different orbital regimes, accuracies achieved by individual techniques, and their limitations.

Characteristics of Radar Measurements

Ground based radar stations can observe objects, when an object is having a flyover within the radar's field of view. Thus re-tracking of an object depends on the ground track repeatability of the orbit. Usual radar observation arc length varies in the range of 50 to 1,000 seconds (1-16 minutes) depending on the altitude and phase of ground track with respect to the observing station.

Radars are the backbone of space surveillance and tracking systems [2], as more than 85% of observations are from radars particularly for LEO objects. Out of which phased array radars constitute for 60% of measurements. In this study, for the purpose of measurement error analysis, only phased array radars are considered. The radars being evaluated here measure range and angles. The radar range measurement error σ_ρ, is defined as the root-mean-square (RMS) of three error components ([7], chapter 8) as in Equation 9

$$\sigma_\rho = \sqrt{\sigma_{\rho N}^2 + \sigma_{\rho F}^2 + \sigma_{\rho B}^2} \tag{9}$$

where the noise range error $\sigma_{\rho N} = \Delta R/\sqrt{2 \cdot SNR}$, SNR being the signal-to-noise ratio, and ΔR is the radar range resolution, which is equal to speed of light divided by two times the signal bandwidth. $\sigma_{\rho F}$ is the fixed random error due to random noise in the receiver and is equivalent to the noise range error at a signal-to-noise ratio of 20dB. $\sigma_{\rho B}$ is the range bias error.

Similar to range measurement error, each angular measurement ($A = \{\alpha, \beta\}$) is characterized by RMS errors of the three components, as in Equation 10

$$\sigma_{A_i} = \sqrt{\sigma_{A_i N}^2 + \sigma_{A_i F}^2 + \sigma_{A_i B}^2} \tag{10}$$

where the angle noise, $\sigma_{A_i N} = B_w/(1.6 \cdot \sqrt{2 \cdot SNR})$, B_w is the radar beamwidth. σ_{AF} is the fixed random error, which will limit angular accuracy.

Usual operational SNR and B_w values for radars under space debris detecting or tracking modes are 10 dB and 0.05 deg [21]. This assumes that the station is tracking an object with size greater than 10 cm and at an altitude of 500 km. Using the above information in Equations 9 and 10, the range error is calculated to be $15m$ and angle errors are 0.01 deg. Walsh [21] provides the σ_ρ and σ_A for five radar observatories within USA and Europe, which are presented in Table 1.

Since most of the radar operational data are not available publicly, for the current research the average of σ_ρ = 10m and σ_A = 0.0028 deg (= $10'' = 4.85 \times 10^{-5}$rad) was considered as nominal quality of radar observations for debris cataloguing. These values are later used for understanding the behaviour of the DSST-OD.

Copyright © 2016 Advanced Maui Optical and Space Surveillance Technologies Conference (AMOS) – www.amostech.com

Tab. 1. Radar measurement errors for openly available radars with maximum sensitivity mode (SNR = 10dB)

	Range error [m]	Angle error [deg]
FPS-85	33.0	0.180
Haystack	0.03	0.008
HAX	0.02	0.014
TIRA	0.50	0.070
DON-2N	10.0	0.037

Characteristics of Optical sensors

An optical sensor, a telescope, tracks satellites across the sky by recording the right ascension and declination. The sensor is composed of a detector (Charge Coupled Device (CCD)), optics, and gimbal. The gimbal is a mounting device which stabilizes the sensor and provides control of the tracking motion.

Detection and tracking from optical sensors rely on the reflected sunlight from the space objects, images captured from CCD sensors are processed to extract astrometric observations in terms of angles (α and β). Accuracy of the derived quantities depend on several factors [12]. A list of the common error sources in optical measurements are presented below and Table 2 provides the magnitude of three telescopes around the globe.

1. Pixel size of a CCD sensor
    - Describes the area of the sky scanned by a single pixel.
    - First order of approximation for accuracy computation: Field of view divided by the number of pixels (average is considered as $3''$).
2. Seeing
    - Describes the effect of the air turbulences on the measured position.
    - After exposure time, light from stars or objects are detected not by a single pixel, but distorted into a two dimensional Gaussian distribution with seeing as standard deviation.
3. Tracking mode
    - Tracking error is dependent on the tracking velocity. An error in tracking velocity makes stars or objects as streaks rather than point-like which induces inaccuracies in deducing angle measurements.
    - Leads to elongated two dimension Gaussian distribution, which in turn is quantified as white noise within measurements.
4. Pointing accuracy
    - Dependent on the accuracy of the mount, when arriving at given direction.
5. Atmospheric corrections
    - Refraction due to atmosphere can lead to wrong angular measurements, hence the line of sight vectors are corrected using atmospheric models.
    - Wrongly applied atmospheric model leads to deviation of extracted quantities.
    - Given the sophistications adapted in reducing the atmospheric effects, the error induced by this effect is assumed to be zero.
6. Gimbal
    - Vibrations due to the motion of the mount leads to errors in measurements.
    - For well balanced telescopes, decay time of the vibrations are small (in the order of few seconds). Taking the advantage of this stabilization, telescopes are planned to point at planned directions ahead of exposure times. Hence, this error source can be neglected, assuming the practice of telescope operations.

Copyright © 2016 Advanced Maui Optical and Space Surveillance Technologies Conference (AMOS) – www.amostech.com

Tab. 2. Operating accuracies of three different telescopes and mounts which are parts of the ZimSMART network [12]

Telescope	Mount	Pixel scale	Seeing	Tracking accuracy	Pointing Accuracy
Takahashi	Paramount	$3.6''$	$2''$	$1'' - 7''$	$10'' - 30''$
ASA	ASA	$1.8''$	$2''$	$0.35'' - 1''$	$\leq 12''$
Takahashi	ASA	$3.6''$	$2''$	$0.35'' - 1''$	$\leq 12''$

Using the average values from Table 2 and computing the RMS value of all the uncertainties, $\sim 15''$ is assumed to be an average error in angular measurements from optical sensors. Given the operational principles and mechanical limitations of a gimbal, ground based optical telescopes are presently used to detect and monitor MEO and GEO objects. An uncertainty of $10''$ in azimuth translates to $50 - 1,200$ [m] in along track direction, and similar range of error in normal direction is considered for further analysis.

Space based sensors

These sensors operate under visible or infrared wave-lengths, that is usually a telescope or an infrared camera. Space based sensors have the ability to detect debris, satellites, and other natural objects orbiting the Earth without being influenced by weather or atmospheric conditions. Also, it has an advantage of higher resolution because of the smaller distance between the observer and the object.

The Midcourse Space Experiment (operational from 1996 - 2006) is one of the space missions dedicated to observe space debris [9], which used an optical sensor to detect small to mid sized debris in the GEO region. The costs of space based sensors are in general higher than the costs of ground based sensors which hinder the launch of new missions. Although, the paper [4] has suggested of using star-tracker on board for the purpose of space situational awareness, it is still not operational on mission level. Therefore, these sensors are left out of the detailed analysis for their error sources. Tables 3 and 4 summarize the observation methods and their accuracies.

Tab. 3. Possible observation methods from different bases employed in LEO (L), MEO (M), and GEO (G) regions for tracking and detecting space objects (*GPS, SLR, Star-tracker)

	Sensor type			
Sensor base	Optical	Radar	Infrared	Others*
Ground	M G	L M	–	–
Space	L M G	–	L M	–
On-board	M G	–	–	L M G

Tab. 4. Average sensor accuracies of optical and radar observation methods

Sensors	Range error (σ_ρ) [m]	Angle error (σ_α, σ_β) [deg]
Radar	10	1.5×10^{-3}
Optical	–	2.8×10^{-3}

To understand the behaviour of typical radar observations, a study was carried out on CAN-X cube-sat satellite observations set. The data set is the part of observation campaign from the TIRA station in Wachtberg, Germany. First plot (left) in the Figure 5 shows the range residuals as a function of observed elevation. It is evident from the figure that range degrades along the slant angles. The intuitive explanation for the behaviour is the Ionospheric refraction imposed on the radar observations. By establishing the ionospheric refraction corrections to range measurements using the observed TEC (Total Electron Content), range-bias as function of elevation can be computed.

Copyright © 2016 Advanced Maui Optical and Space Surveillance Technologies Conference (AMOS) – www.amostech.com

The red line curve in the Figure 5 shows bias function for the considered test case. The observed random range residual errors are also scaled along elevation. This needs further investigation considering larger data sets from different sources in order to generalize the behaviour.

Centre and right plots in the figure 5 shows the elevation and azimuth residuals for the same set of observations as a function of observed elevation. Similar to range residuals behaviour the elevation residuals too exhibited larger residuals at lower elevations than at higher observed elevations. Also, the detailed inspection shows the directional separation in the residuals. That is the observations on east had different peak than that of the observations obtained pointing to west. This too requires further investigation to establish the general correlation.

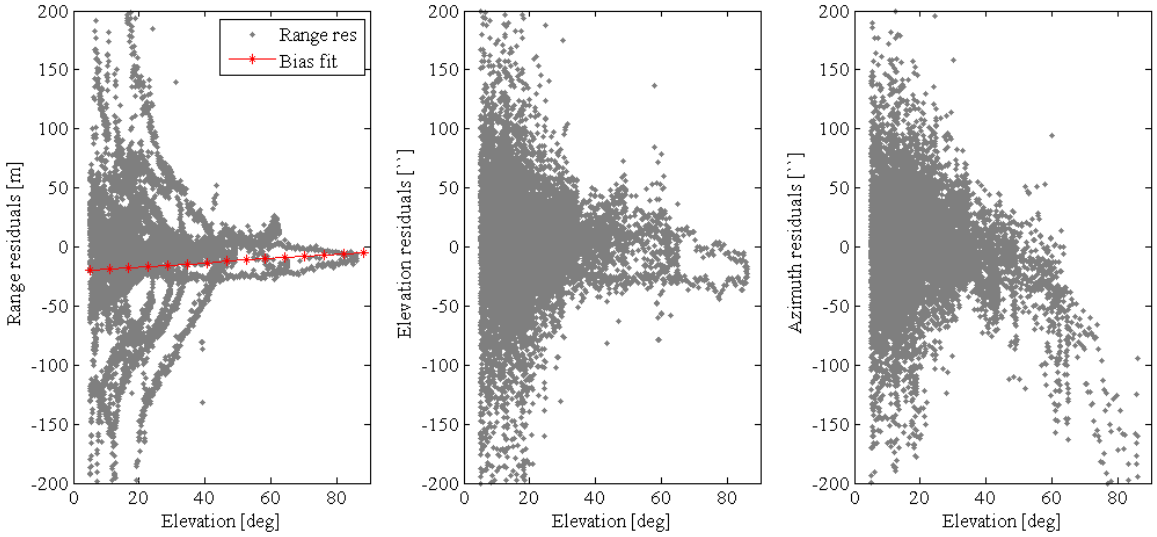

Fig. 5. CAN-X radar observation's (left) range residuals, (middle) elevation residuals, and (right) azimuth residuals as a function of observed elevation. Observations used in orbit estimation are between dates 23.02.2012 - 03.03.2013

Due to the lack of availability of raw observation sets of different satellites, stations, and time period, this study could not be concluded with concrete remarks. But, the authors intend to investigate and characterize the observations as a part of the future study. The present results also shows that the elevation dependent weighting within a least square orbit estimation procedure might lead to more accurate orbit estimations.

4. PRIMARY INVESTIGATION ON ORBIT PREDICTION ACCURACY OF DSST

Previously in our study [19], we tested the fit accuracy of the DSST in comparison to a numerical propagation method. During the test the reference orbits were generated using Adam-Bashforth integrator with high-fidelity force models: 50×50 geopotential terms, sun and moon point masses, Jacchia-Gill density model, and cannonball solar radiation pressure model. This test showcased that the DSST is capable of imitating the cowell trajectories with the accuracy of five to ten meters for seven day propagation lengths, in LEO, MEO, and GEO. For highly eccentric orbits the DSST was able to propagate with the accuracy range of 50 to 100 meters.

In the present section we emphasize on the prediction accuracy of the DSST. In order to obtain the general prediction behaviour of the selected semi-analytical method, we assume that the numerically generated orbits provide the best possible reference trajectories (as an alternative to real observations). The employed test methodology is as follows:

1. A reference trajectory was generated using above mentioned numerical propagator for seven plus N number of days.
2. A set of DSST mean-elements are estimated for the first seven days' reference trajectory.

Copyright © 2016 Advanced Maui Optical and Space Surveillance Technologies Conference (AMOS) – www.amostech.com

3. Estimated mean-elements are then propagated using DSST.
4. The propagated ephemeris are compared against the reference ephemeris at N number of days.
5. Position differences are measured as comparison metrics.

Figure 6 shows the position differences of DSST against numerical orbits for different prediction lengths and at different altitudes. These tests provide the insight on the degradation of orbits while propagating the mean-element sets. The position accuracy is lower and degrades faster at the semi-major axis below 6900 km. Intuitively, this is imputed to higher drag perturbations at these altitudes. Similar tests performed in MEO and GEO regions showed that the position differences remained below 15 meters for the prediction lengths of up to 21 days.

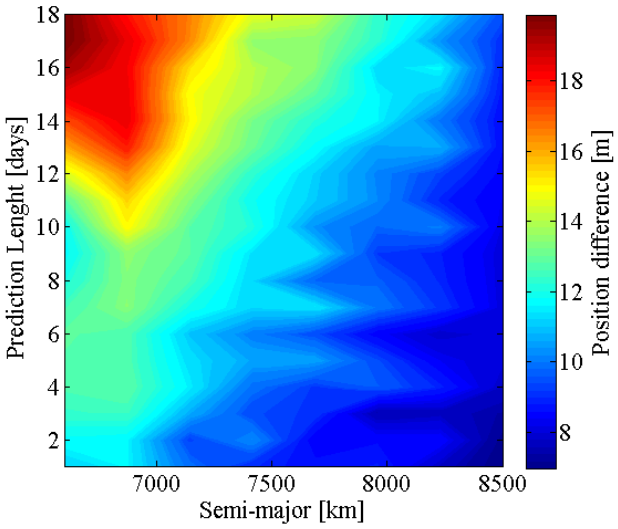

Fig. 6. Position differences between DSST and cowell orbits, at different altitudes and for different prediction lengths in LEO regime

The major limitation of the test methodology is that, the atmospheric densities are computed using the Jacchia-Gill density model in both propagators (generating reference trajectories and DSST predictions). This restraints from obtaining the actual information on real-world prediction accuracies in LEO region. Equivalently, in higher altitudes, MEO and GEO orbits, the non-conservative solar radiation pressure was computed using same radiation pressure models. In order to obtain actual insight on prediction accuracies, we intend to make use of the real observation data for our future studies.

5. FACTORS INFLUENCING THE ACCURACY OF THE ORBIT ESTIMATION

In general, the accuracies of the estimated orbit depends on several factors, such as:

1. Geo-potential model differences
2. Atmospheric model errors
3. Computational errors
4. Geometric distribution of observations
5. Accuracy of the partial derivatives
6. Measurement errors
7. Coordinate reference errors

Copyright © 2016 Advanced Maui Optical and Space Surveillance Technologies Conference (AMOS) – www.amostech.com

Geo-potential, atmospheric-model, and computational errors are dependent on models used and the propagation technique. Each of these error sources require individual attention and detailed investigations. In the present study they are assumed to be near zero, and we proceed further to analyse the effects of observations. Following subsections present the influence of distribution of observations on mean element estimation followed by orbit determination with noisy and biased data. In the end we present the analysis on the radius of convergence, in turn partial derivatives which are used within DSST-OD.

5.1. Observability / Time distribution of observations

Figure 7 shows the fit residuals for PROBA-V satellite data in radial, tangential and normal directions. The Figure presents fit residuals from three orbit estimation runs with:

- "cont. obs" - continuous data of positions in ITRF through GPS observations for the span of seven days with one minute interval (7721 observations)
- "sparse obs 1" - sparse data set includes 450 observations over the seven day arc which are observed once per revolution, and
- "sparse obs 2" - sparse data set includes 150 observations which are observed from the same station on uneven intervals over the span of seven days.

Similarly, observations of a GNSS satellite were created with:

- "cont. obs" - continuous data of positions in ITRF for the span of ten days with three minute interval (5040 observations)
- "sparse obs 1" - sparse data set includes 70 observations, and
- "sparse obs 2" - sparse data set includes 30 observations.

These data sets were designed to mirror the SSA-type tracking conditions. That is five to ten minutes of dense observations per orbit, and repeatability is not homogeneous due to observability conditions. The fit statistics for these cases in comparison with numerical-fit are presented in Table 5.

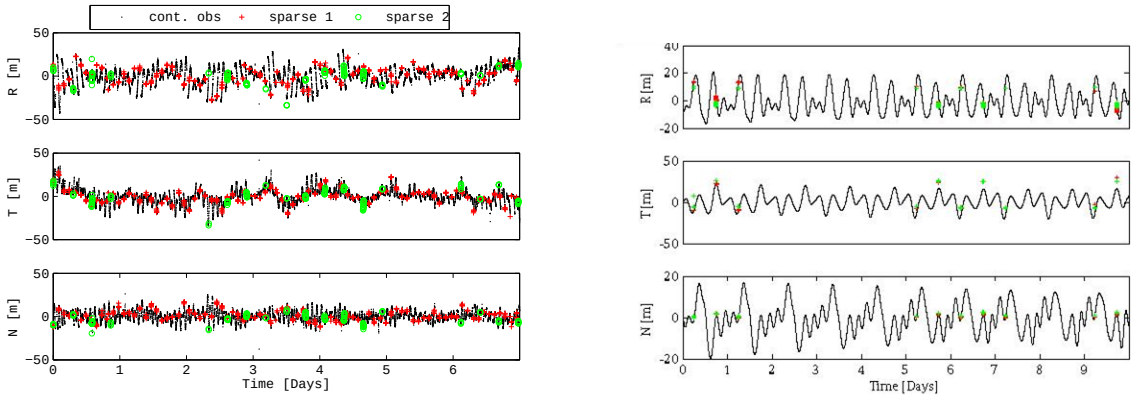

Fig. 7. R-T-N fit residuals from DSST-OD to (left) PROBA-V and (right) GNSS fit residuals. Observation epoch starts at 00:00:30, January 01, 2014. Figure shows fit residuals for three sets of data described in the text

Since the numerical method uses osculating element space for propagation, it is expected to converge at same set of epoch elements irrespective of the spatial and time distribution of the observations. But, the DSST makes use of averaged orbits and the mean element set is estimated. This in turn makes the spatial distribution of observations to influence the accuracy of epoch elements. From Table 5 and Figure 7 it is observed that the geometrically biased observations, counter intuitively, did not have any significant effect while estimating the orbits using DSST. This

Copyright © 2016 Advanced Maui Optical and Space Surveillance Technologies Conference (AMOS) – www.amostech.com

Tab. 5. DSST and ODEM orbit determination statistics for PROBA-V and GNSS observations

		Proba-V				GNSS			
Obs type		Radial [m]	Along-track [m]	Cross-track [m]	Position RMS [m]	Radial [m]	Along-track [m]	Cross-track [m]	Position RMS [m]
DSST-OD									
cont. obs	RMS	10.83	8.79	6.20	15.26	5.65	11.31	4.22	13.32
	Mean	0.03	0.12	0.55		0.01	0.01	0.03	
sparse obs 1	RMS	10.22	8.17	6.08	14.43	5.81	10.83	4.03	12.93
	Mean	0.25	-0.36	1.11		0.05	1.85	3.72	
sparse obs 2	RMS	8.69	8.70	7.44	13.79	4.19	8.80	3.62	10.54
	Mean	-0.36	-0.09	-3.12		0.56	2.09	4.48	
Numerical - OD									
cont. obs	RMS	2.59	6.92	1.56	7.79	1.44	5.12	2.70	5.96
	Mean	1.77	0.01	0.79		0.54	0.01	0.79	
sparse obs 1	RMS	2.76	6.44	1.58	7.62	1.76	4.91	1.65	5.47
	Mean	1.86	0.01	0.25		0.58	0.08	0.25	
sparse obs 2	RMS	2.46	7.01	1.23	7.53	1.59	4.20	1.15	4.63
	Mean	1.91	0.08	0.93		0.69	0.01	0.93	

proves that the DSST is capable of recovering the short-periodic perturbations to relevant accuracy in order to estimate the right set of mean elements. This assumes that the provided a-priori used to initialize the OD program is within the radius of convergence.

The difference between the orbit estimated using continuous data set and sparse data for PROBA-V case did not show any significant deviations, as one would expect with an analytical or a semi-analytical theory. But, when comparing the true orbit of a GNSS satellite and the orbit estimated using "sparse obs 2" case (30 observations), the position RMS was observed to deviate over 50 meters. This is an order higher than the DSST's prediction accuracy for GNSS satellites or the quality of the observations used.

5.2. Observation noise and bias

The orbit determination program estimates epoch elements by computing the residuals between measured quantities and computed quantities. Generally, any measurement system is corrupted by various noises (electronics, atmosphere, process, etc.), and with or without bias in the observations. Hence, the output of an OD program is also limited by accuracy of the observations. This section provides an overview of the analysis performed to evaluate accuracy of estimated orbits while using simulated observations.

Figure 8 illustrates the method adapted in simulating observations and then comparing the accuracy of the estimated orbits. This method was employed to understand the influence of observation errors on orbital errors.

Figure 9 (left) shows the radial, in-track, and normal error components of the estimated orbits. As the noise and bias in an angular measurement (azimuth) increases, the error in in-track component was seen increasing. Similar behaviour was noted when observed elevation was distorted. The radial component error was not driven by the noise in angular observations. Hence, the noise and biases in angular measurements translated mainly into in-track (satellite position or mean-anomaly) errors in the estimated orbits. That is to say that, one could obtain accurate orbit information from noisy angular measurements, but the certainty in the position information is lost.

When radial component was biased and corrupted with random noise, both the orbit and position information were not retrieved. Figure 9 (right) shows the difference between true and estimated orbits at different altitudes while using 10 m bias and 5 m one sigma noise in range measurement, and 10 arc seconds bias and 5 arc seconds noise in azimuth and elevation measurements. It is observed that, the range and angular measurement errors influences the position uncertainty in lower orbits, while the same error sources influence the orbital shape parameters at higher altitudes.

Copyright © 2016 Advanced Maui Optical and Space Surveillance Technologies Conference (AMOS) – www.amostech.com

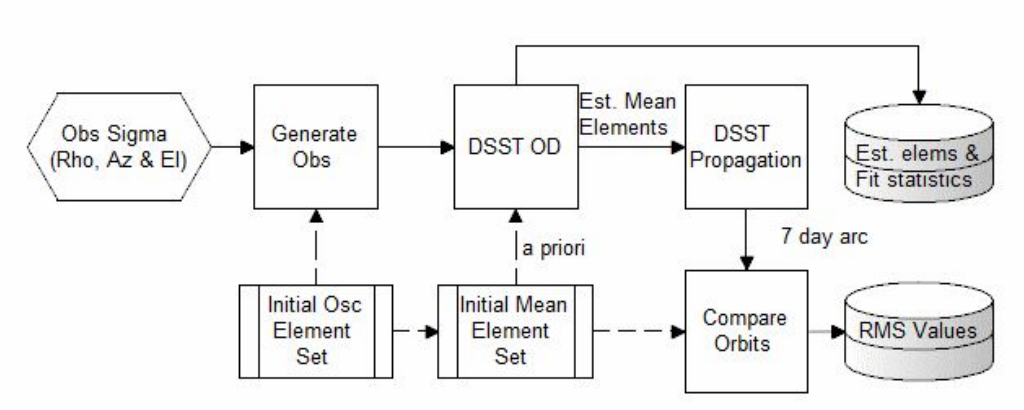

Fig. 8. Flow chart for the observation simulation scheme for analysing the performance of OD system.

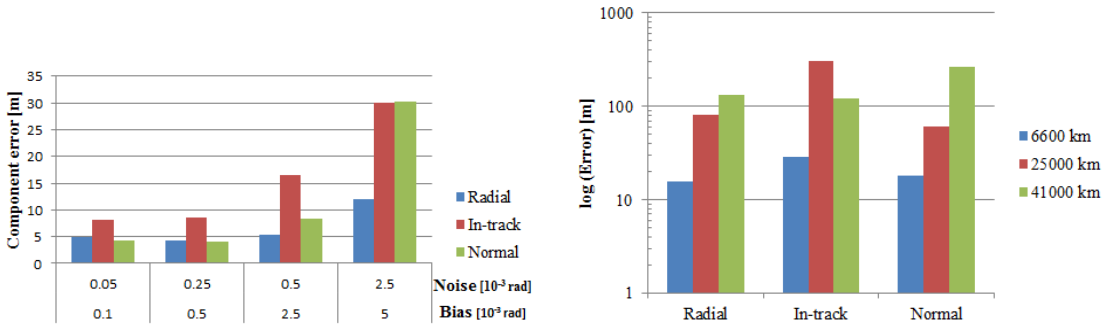

Fig. 9. (left) Shows the behaviour of RMS error for a PROBA-V orbit fits for increasing level of noise and bias in observations. (right) Shows the behaviour of radial, in-track, normal components error at different altitudes using 10 m bias and 5 m one sigma noise in range measurement, and 10 arc seconds bias and 5 arc seconds noise in azimuth and elevation measurements

Copyright © 2016 Advanced Maui Optical and Space Surveillance Technologies Conference (AMOS) – www.amostech.com

In conclusion, the simulation tests showed that the noisy observational data influence position or shape parameters at different altitudes.

5.3. Radius of convergence

The orbit determination program generally computes residuals between measured quantities and estimated quantities, and determines the parameters by minimising the square root of the sum of the squared residuals. The direction for the convergence is provided through the partial derivative matrices, which is the slope directing the iterations towards the minima. The partial derivative matrix are computed either by integrating the variation of parameter equations or by using finite difference method. As explained in the section 4 of the paper, the present DSST-OD program makes use of the partial derivatives which are approximated by using the averaged variation of parameter equations. On top of which the short-periodic J2 partials are analytically computed. Previously it has been shown [19] that, just the J2 partials are sufficient for the convergence and finding the global minima. This section presents the test cases those were conducted in order to answer the question: how far can be the a-priori orbit used to initialise the OD.

Tab. 6. A-priori and converged elements from radius of convergence test on a LEO satellite. The table presents biased semi-major test case

	Initial a-priori	Converged orbit	RMS diff
Exact or True a-priori	0.**69277159**E+04 0.16422515E-02 0.82384702E+02 0.17198184E+03 0.54493609E+02 0.16115461E+03	0.6927715**984**E+04 0.164**2251569**E-02 0.8238**470287**E+02 1.7198184**547**E+02 0.544**9360972**E+02 1.611**5461056**E+02	1E-10 [m]
Semi-major biased with 0.5 m	0.**69277109**E+04 0.16422515E-02 0.82384702E+02 0.17198184E+03 0.54493609E+02 0.16115461E+03	0.6927715**981**E+04 0.164225156**3**E-02 0.823847**0281**E+02 1.7198184**546**E+02 0.5449360272E+02 1.611546102**6**E+02	1E-6 [m]
Semi-major biased with 10 km	0.**6937**7159E+04 0.16422515E-02 0.82384702E+02 0.17198184E+03 0.54493609E+02 0.16115461E+03	0.6927715**797**E+04 0.164**1574491**E-02 0.823847**1591**E+02 1.7198184**307**E+02 0.544**7998329**E+02 1.611**6803776**E+02	7.62 [m]
Semi-major biased with 50 km	0.**6977**7159E+04 0.16422515E-02 0.82384702E+02 0.17198184E+03 0.54493609E+02 0.16115461E+03	0.7027966832E+04 0.2070711543E-02 0.8827644293E+02 0.1782077399E+03 0.4885912183E+02 0.2446790427E+03	1E+6 [m]

Table 6 presents the convergence test cases with biased a-priori semi-major axis. It shows that the DSST-OD converged at different minima depending on the a-priori mean-element sets. In the second row, when semi-major is biased with 0.5 meters, it is observed that the converged solutions found the minimum in-line with the iteration stopping criterion. In third case, when semi-major is biased with 10 km, the estimated orbit diverged from the true orbit by 7.62 m. From brute force simulations, it was observed that DSST-OD found the true minima when the semi-major axis was biased up to ±5 m, for this perticular test orbit, and the secondary minima, where the estimated orbit deviated from the true orbit by $\sim$ 7.5 m, was achieved with biasing up to ±30 km. When the a-priori is biased beyond this point, the DSST-OD failed to converge to right orbital parameters. By detailed analysis, the behaviour of two minima points could be explained with the use of analytical J2 partial derivatives. When finite difference partial derivatives were used, this behaviour did not occur.

Similar biasing simulations were carried out for other orbital elements, and it was observed that the same orbits were achieved depending on the extent of the a-priori bias. Example: when eccentricity was biased with 1E-7, it found the same orbit as semi-major biased with 0.5 m. When the eccentricity was biased with 1E-5, it found the same orbit as semi-major axis biased with 10 km.

The behaviour of radius of convergence is also dependent on the type of observations processed and the type of estimated epoch elements set. With the similar simulation method, it was also observed that estimating mean

Copyright © 2016 Advanced Maui Optical and Space Surveillance Technologies Conference (AMOS) – www.amostech.com

equinoctial element set has the radius of convergence one order of magnitude greater than that of estimating position and velocity at epoch.

Table 7 shows the added advantage of estimating mean equinoctial elements, in terms of number of iterations, in comparison with determining positions and velocities.

Tab. 7. Batch least square estimator performance when estimating epoch elements in different coordinate systems

Coordinate type	Initial RMS [m]	Iteration 2 RMS [m]	No. iterations	Final RMS [m]
Cartesian elements	25350	14200	7	9.13
Mean Equinoctial elements	25350	593	4	9.13

The simulations provide the insight in to the extent of using the a-priori information within DSST-OD. This also appends the usability of DSST as a satellite theory for the purpose of space object catalogue maintenance system. The advantages come from the fact that, the mean equinoctial elements behave as a linear oscillator. Which reduces the non-linear dynamics within the modelled system.

6. CONCLUSIONS

The study summarizes the accuracy of different observation methods, which are dedicated for a space object catalogue maintenance system. By understanding the technical and operational limitations of optical and radar observations methods, it has been established that the average observation errors are in the order of 10-50 m, depending on the altitude of the observed object. An implemented semi-analytical partial derivative computation, which makes use of Draper Semi-analytical Satellite Theory, has been successfully tested within a least square orbit determination program. Errors within the observations, their possible SST way of observation flow to a catalogue maintenance system, and other aspects concerning the accuracy of mean element estimation have been tested using both simulated and real observations.

The prediction accuracy of DSST is discussed in brief. By comparing the DSST predicted orbits to more accurate numerically generated orbit, we have observed that the DSST propagates the orbits with accuracies well below the observation accuracies, that flows into a catalogue maintenance system.

Later, different attributes such as:

- Influence of geometrical and time distribution of observations on estimating mean elements
- Influence of bias and noise in the observations
- Influence of the a-priori states on the estimated orbits

are discussed in context of estimating DSST mean elements.

The sparse distribution of observation test cases showed that DSST is capable of recovering short-periodic perturbations to required catalogue maintenance accuracies. The same tests also established that the estimated mean element sets do not deviate farther than the propagation accuracy of the technique. This provides an added advantage over other analytical methods, and computationally over numerical method. Test cases involved in establishing radius of convergence for a-priori used to initialize DSST-OD showed that, J2 partials is sufficient for obtaining the convergence. Together with, propagating and estimating mean element sets have added advantage of faster convergence and larger a-priori uncertainty within least square orbit determination procedure.

The major limitation of the present study is, that the performed analysis suffers from the very limited observation data sets. Though it provided the high-level overview of a orbit determination programs behaviour, it requires intense analysis to gain further insights and to establish concrete astrodynamical explanation.

Copyright © 2016 Advanced Maui Optical and Space Surveillance Technologies Conference (AMOS) – www.amostech.com

7. FUTURE WORK

To over come the limitations of the present study, the future works is planned to perform the similar investigations using larger-real-observation sets. Along with which, authors propose to perform further research and implementation works in the following directions:

- Improving the observation weighting scheme within DSST-OD as a function of observed elevation.
- Inclusion of GNSS observations in GTDS sensor datasets.
- Performing the attribute tests with ISON data sets.
- Establish the actual a-priori limitations as function of altitude and eccentricity.

ACKNOWLEDGEMENT

The work was funded by the Munich Aerospace scholarship program. The authors would like to thank Dr. Kirschner, and Dr. Montenbruck for providing CAN-X and PROBA-V observation data sets.

8. REFERENCES

1. Barker, W. N., Casali, S. J., Walker, C. H. Improved Space Surveillance Network Observation Error Modeling and Techniques for Force Model Error Mitigation. AAS/AIAA –Astrodynamics Specialist Conference. Girdwood, Alaska, 16-19 August, 1999.
2. Berger, J. M., Moles, J. B., and Wilsey, D. G., An Analysis of USSPACECOM's Space Surveillance Network (SSN) Sensor Tasking Methodology, Air Force Institute of Technology, Faculty of the School of Engineering, Master Thesis. 1992.
3. Boikov, V. F., Makhonin, G. N., Testov, A. V., Khutorovsky, Z. N., and Shogin, A. N., Prediction Procedures Used in Satellite Catalog Maintenance. Journal of Guidance, Control, and Dynamics. DOI: 10.2514/1.41488.
4. Boyle, D. R., Mortari, D., and Pollock, T. Use of Star Trackers for Space Situational Awareness, Space Control Conference, MIT Lincoln Laboratory, Lexington, MA. 2006
5. Broucke R. A., and Cefola P. J., Equinoctial Orbit Elements - Application of Artificial Satellite Orbits, Astrodynamics Specialist Conference 72-937, Palo Alto, CA, USA. September 1972.
6. Cefola, P. J.,A Recursive formulation for the Tesseral Disturbing Function in Equinoctial Variables, Astrodynamics Specialist Conference, San Diego, CA, USA. August 1976.
7. Curry, G. Richard, Radar system performance modeling,ISBN: 9781580538176, Artech House radar library series, 2005.
8. Cefola, P. J.,Sabol, C., Hill, K., and Nishimoto, D., Demonstration of the DSST State Transition Matrix Time-Update Properties Using the Linux GTDS Program, Proceedings of the Advanced Maui Optical and Space Surveillance Technologies Conference, held in Wailea, Maui, Hawaii, p.E35, September 2011.
9. Egan, M. P., Price, S. D., Wright, C. O., and Mizuno, D. R. The Midcourse Space Experiment Point Source Catalog Version 2.3 Explanatory Guide. Air Force Research Laboratory. 2013.
10. ESA, Space Surveillance and Tracking-SST Segment, http://www.esa.int/Our_Activities/Operations/Space_Situational_Awareness/Space_Surveillance_and_Tracking_-_SST_Segment, European Space Agency, February 2014.
11. Green, A. J., Orbit Determination and Prediction Process for Low Altitude Satellites, Doctoral Thesis, Department of Aeronautics and Astronautics, Massachusetts Institute of Technology, December 1979.

Copyright © 2016 Advanced Maui Optical and Space Surveillance Technologies Conference (AMOS) – www.amostech.com

12. Herzog, J., Cataloguing of Objects on High and Intermediate Altitude Orbits. Doctor of Philosophy, Bern, Switzerland. Astronomisches Institute der Universitaet Bern. 2013.

13. McClain, W. D., A Recursively Formulated First-Order Semi-analytic Artificial Satelllite Theory based on the Generalized Method of Averaging. Vol. I, Tech. Report CSC/TR-77/6010, Computer Sciences Corporation, 1977.

14. McClain, W. D., A Recursively Formulated First-Order Semi-analytic Artificial Satelllite Theory based on the Generalized Method of Averaging. Vol. II, Tech. Report CSC/TR-78/6001, Computer Sciences Corporation, 1978.

15. Montenbruck, O., Gill, E., Satellite Orbits: Models, Methods, and Applications Second print, Springer-Verlag Berlin Heidelberg New York,ISBN: 3-540-67280-X, 2001.

16. Morton, M. M., and Roberts, T., Joint Space Operations Center (JSpOC) Mission System (JMS). In : Advanced Maui Optical and Space Surveillance Technologies Conference. Maui, USA, 12-16 September. AMOS. 2011.

17. NASA Orbital Debris Porgram Office: Orbital Debris. Quaterly News. National Aeronautics and Space Administration. April, 2016.

18. Seago, J. H., Griesbach, J., Woodburn, J. W., and Vallado, D. A. Sequential Orbit-Estimation with Sparse Tracking. AAS/AIAA Space Flight Mechanics Meeting. New Orleans, Louisiana, 13-17 February. 2011.

19. Setty, S. J., Cefola, P. J., Montenbruck, O., and Fiedler, H. Application of Semi-analytical Satellite Theory Orbit Propagator to Orbit Determination for Space Object Catalogue Maintenance. Advances in Space Research. 2015.

20. Vallado, D. A., Fundamentals of Astrodynamics and Applications, Second Edition, ISBN: 1-881883-12-4, 2001.

21. Walsh, D. W., A Survey of Radars Capable of Providing Small Debris Measurements for Orbit Prediction, 2013.

22. Wiedemann, C., Flegel, S. K., Gelhaus, J., Krag, H., Klinkrad, H., and Vörsmann, P., NaK release model for MASTER-2009. DOI: 10.1016/j.actaastro.2010.10.014. 2011.

Copyright © 2016 Advanced Maui Optical and Space Surveillance Technologies Conference (AMOS) – www.amostech.com